# EFFICIENT STATION-KEEPING FOR CLUSTER FLIGHT

**Dr. Matthew C. Ruschmann**(1)**, Dr. Brenton Duffy**(2)**, Rafael de la Torre**(3)**, and
Dr. Sun Hur-Diaz**(4)

(1),(2),(3),(4)*Emergent Space Technologies Inc., 6411 Ivy Lane, Suite 303, Greenbelt, MD 20770*
*(301) 345-1535*
(1)*matthew.ruschmann@emergentspace.com*
(2)*brenton.duffy@emergentspace.com*
(3)*rafael.delatorre@emergentspace.com*
(4)*sun.hur-diaz@emergentspace.com*

***Abstract:*** *A key challenge of guidance, navigation, and control for clustered satellite flight is long duration station-keeping of the cluster. The secular perturbations that force the cluster to drift apart must be corrected periodically, and the satellites must maintain safe relative orbits. Ideally, the station-keeping would be semi-autonomous to the point that the ground crew required for the mission is similar to that required for a traditional monolithic satellite performing the mission. A unique strategy is developed that efficiently maintains the cluster by using control boxes in the relative frame. Several alternative cluster station-keeping strategies are discussed as well. Their performance is analyzed over 500 orbits using a high-fidelity simulation with GPS navigation. The strategies are down-selected based on the results of this trade study and implemented into flight software for DARPA's System F6 (Future, Fast, Flexible, Fractionated, Free-Flying Spacecraft United by Information Exchange) program, which seeks to address the challenge of developing future space systems via fractionated architectures wherein wirelessly networked modules would communicate, collaborate and share resources to accomplish their mission.*

***Keywords:*** *System F6, cluster flight, station-keeping, receding horizon control, guidance, control box, GN&C*

## 1. Introduction

Efficient station keeping is a key challenge of guidance, navigation, and control for clustered satellite flight [1]. Secular perturbations, such as forces due to a non-spherical Earth and atmospheric drag, pull modules in the cluster apart and must be corrected periodically by maneuvers [2]. The corrections not only require fuel, but can also demand attitude changes that may interrupt the mission's objectives. This paper develops multiple station keeping strategies for clustered flight, and performance criteria for efficient station keeping are defined to evaluate the strategies. A Monte Carlo analysis is conducted to quantify the performance of each strategy. The most efficient strategy is down-selected for implementation into flight software.

Station keeping and control of multiple spacecraft in clusters has long been studied. Early research into cluster flight investigated proximity operations for rendezvous [3]. More recently, there is interest in long-term maintenance of a cluster that cooperate to achieve a common goal [4, 5]. Some missions require the modules to maintain a specific formation. If a formation is not required, the cluster still needs to avoid collisions while keeping nearby one another for wireless communication. The flocking controller maintains passive safety and an upper bound on inter-module distance

while allowing the modules to drift freely otherwise [6]. The flocking controller defines passive safety using relative orbit elements (ROEs), which were first introduced for formation keeping by Lovell [7]. ROEs are also the basis of the contracting controller, which is not efficient but has guaranteed convergence [8]. Other research has shown that specifying the formation as variations in Keplerian orbital elements (VKOE) is more accurate for clusters with large separation [9]. Although the strategies in this paper use ROEs to define the geometry of the cluster, the methods could be adapted to define the geometry using VKOEs. A two burn correction of VKOEs for formation keeping was developed by Vadali [10], which was adapted for the PRISMA mission [11]. VKOEs have also been used to formulate receding horizon control (RHC) for formation keeping [9].

The station-keeping strategies developed in this paper build on the concept of RHC. RHC repeatedly solves an optimal control problem over a finite time window [12]. In spite of being developed for constrained problems without analytical solutions, RHC has proven performance and stability for nonlinear systems under different sets of assumptions [13]. RHC has seen practical applications for industrial settings in which constrained systems are common. There has also been recent research into RHC for formation keeping of satellite systems [9]. In addition, RHC was investigated for an application to proximity operations during a Mars return scenario [14].

Three strategies are developed in this paper and analyzed with various tuning configurations. The first strategy is RHC in its standard formulation. The other two strategies are modifications to RHC that preclude the generic proofs of stability but significantly improve the performance of long-term station-keeping. The first modification is the addition of control regions to the RHC strategy, which are specified using ROEs. This strategy reduces the frequency of burns by updating maneuver plans only when necessary to prevent secular drift and maintain passive safety. This approach is similar to the traditional station-keeping control strategy used for geostationary satellites using control box regions. For our station-keeping strategy, the control box concept is applied to ROEs in the relative space. The third strategy is based on modifying the control horizon such that the maneuver window deadline no longer recedes into the horizon.

The trade study in this paper considers the three strategies that are developed as well as the flocking controller. A set of performance metrics for efficient station-keeping is defined for a cluster, related to fuel requirements, burn frequency, and safety. ROE targeting (adapted from reference [7]) and the contracting controller were also investigated, but were down-selected before the Monte Carlo analysis of long duration station-keeping was started due to their performance. The remaining station-keeping strategies were evaluated using Monte Carlo analysis over 40 runs of 500 orbits each, approximately four weeks each. The mean results over 500 orbits were extrapolated to determine the fuel requirements for a nominal six month mission. The efficiency of the strategies was evaluated from the performance metrics.

The results of this study were used to down-select to a single station-keeping strategy, which has been implemented into flight software for DARPA's System F6 (Future, Fast, Flexible, Fractionated, Free-Flying Spacecraft United by Information Exchange) program. System F6 seeks to address the challenge of developing future space systems via fractionated architectures wherein wirelessly networked modules would communicate, collaborate and share resources to accomplish

their mission. This station keeping algorithm is part of Orbit Maintenance Service (OMS) within Cluster Flight Application (CFA) developed by Emergent Space Technologies to provide guidance, navigation, and control for System F6 [15]. Figure 1 is a diagram of OMS responsibilities for guidance and control in CFA. The strategies developed in this paper provide maneuver time windows and specific targets to a robust Maneuver Planning Service (MPS) [16]. OMS relies on the Navigation Service (NAV) for module state estimates [17]. Cluster Flight Manger (CFM) is responsible for managing the frequency of orbit maintenance and distributing maneuver plans to Module Maneuvering Service (MMS). MMS sends maneuver commands to the bus at the appropriate time, which are translated by Module Proxy (MPx).
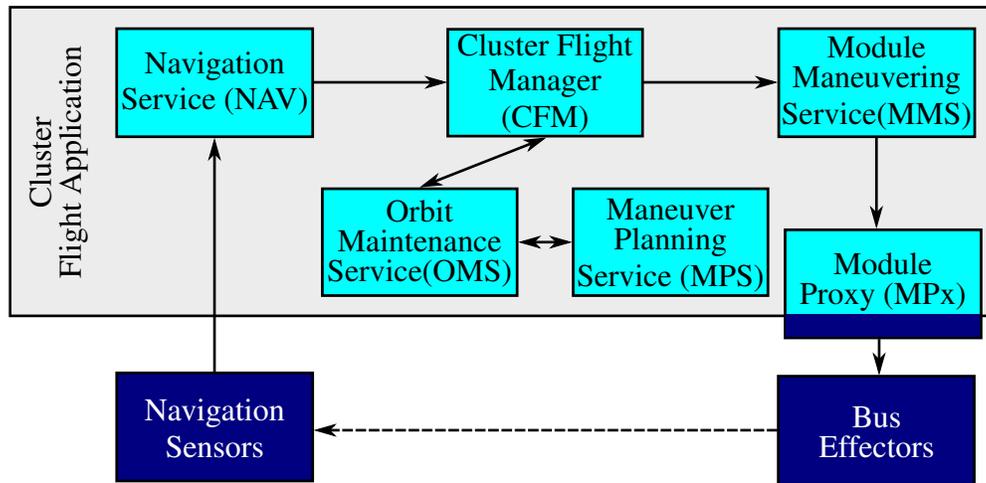


**Figure 1: The role of OMS for guidance and control in the Cluster Flight Application (CFA).**

This paper is organized as follows. Section 1 is this introduction. Section 2 reviews the concept of ROEs and defines passive safety of the cluster in terms of ROEs. The coordinate frames and effects of a non-spherical Earth are also reviewed. Section 3 introduces the station-keeping strategies based on the concept of RHC and ROE control boxes. Design and tuning of the strategies are discussed. Section 4 briefly reviews the concepts and implementation of the flocking controller. Section 5 describes the long-term station-keeping Monte Carlo analysis and presents the trade study results. Section 6 summarizes conclusions from the results and announces the down-selected station-keeping strategy.

## 2. Defining Passive Safety using Relative Orbit Elements

Passive safety ensures that modules are always on trajectories with a low probability of collision in case the propulsion systems on a module fail without advanced notice. We define passive safety in terms of ROEs, as was done by Schwartz [6]. This analysis is done in the absence of perturbations. In this section, we start by reviewing the reference frames used in this paper followed by a brief definition of ROEs and their precession due to a non-spherical Earth. The interested reader should reference Lovell [7] for more information on ROEs.

## 2.1. Frames of Reference

The International Celestial Reference Frame (ICRF) represents absolute positioning relative to Earth. ICRF uses a quasi-inertial coordinate frame centered at the Earth and a set of orthogonal Cartesian unit vectors with the $\bar{z}$ axis pointing through the North Pole. A useful frame for defining the relative motion of two spacecraft is the RSW frame.* RSW is an orthogonal reference frame, often referred to as Hill's frame [18] for circular orbits, centered at the origin of one spacecraft and rotating as it moves around in its reference orbit. Figure 2 demonstrates the geometry of the RSW frame at a single instance in the reference orbit. The $x$ axis (R component) of RSW is defined along the instantaneous position vector in the direction of zenith, which is referred to as the radial axis. The $z$ axis (W component) points in the direction of the orbit angular momentum vector, and is referred to as the cross-track axis. The $y$ axis (S component) completes the orthogonal, right handed coordinate system, which is referred to as the along-track axis because it points along the direction of motion for the orbit. A local vertical curvilinear (LVC) frame is similar to RSW, but the axes curve along the shape reference orbit. The $y$ axis curves along the direction of along-track motion, and the $z$ axis curves along the direction of cross-track motion as demonstrated in Fig. 2. This improves the accuracy of relative orbit propagation for long along-track distances.
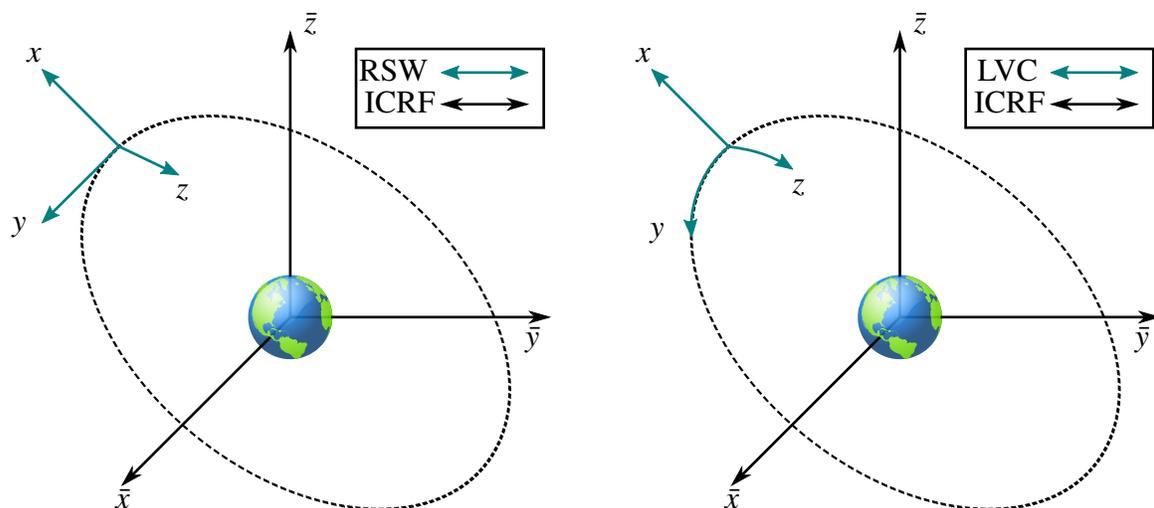


**Figure 2: Diagrams of RSW and LVC with respect to ICRF centered at the Earth's origin at an instance in time. The reference orbit is the dotted ellipse. LVC is an RSW frame with curvilinear along-track axis ($y$) and curvilinear cross-track axis ($z$).**

## 2.2. Relative Orbit Elements

ROEs are a six-tuple ($a_e$, $x_d$, $y_d$, $\beta$, $z_{max}$, $\gamma$) that represents the geometry of a relative orbit in the LVC frame of a reference orbit. The transformation of LVC position and velocity to ROEs is a nonlinear transformation defined by the following functions:

$$a_e = 2\sqrt{\left(\frac{\dot{x}}{\omega}\right)^2 + \left(3x + 2\frac{\dot{y}}{\omega}\right)^2},$$

---

*For circular orbits, the along-track and in-track directions are always the same, so this coordinate frame is sometimes called 'RIC.'

$$x_d = 4x + 2\frac{\dot{y}}{\omega},$$

$$y_d = y - 2\frac{\dot{x}}{\omega},$$

$$\beta = \arctan\left(\frac{\dot{x}}{3\omega x + 2\dot{y}}\right),$$

$$z_{max} = \sqrt{\left(\frac{\dot{z}}{\omega}\right)^2 + z^2},$$

$$\gamma = \arctan\left(\frac{\omega z}{\dot{z}}\right) - \arctan\left(\frac{\dot{x}}{3\omega x + 2\dot{y}}\right) \tag{1}$$

where $\dot{x}$, $\dot{y}$, and $\dot{z}$ are the velocities in the radial, along-track, and cross-track directions, respectively. The inverse transformation also has a functional representation:

$$x = x_d - \frac{a_e}{2}\sin(\beta),$$

$$y = a_e \sin(\beta) + y_d,$$

$$z = z_{max}\sin(\gamma + \beta),$$

$$\dot{x} = \frac{a_e}{2}\omega\sin(\beta),$$

$$\dot{y} = a_e\omega\cos(\beta) - \frac{3}{2}\omega x_d,$$

$$\dot{z} = z_{max}\omega\cos(\gamma + \beta)$$

The geometric interpretation of ROEs is the key to their usefulness. Figure 3 and later in Fig. 4 diagram the geometric meaning of ROEs in LVC.



(a) When $x_d = 0$ the relative orbit is a closed and repeating in the x-y plane.

(b) When $x_d \neq 0$ the relative orbit is open and drifts along the y axis (along-track).
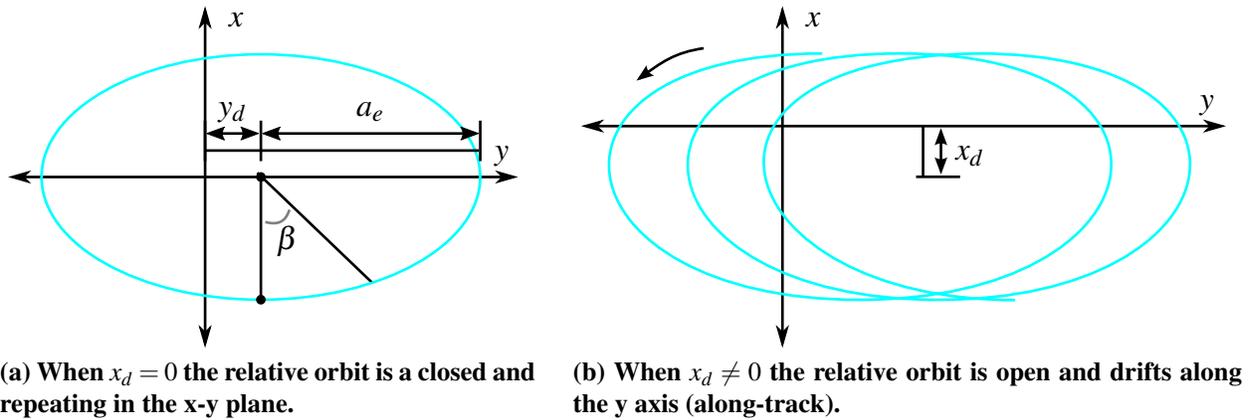
**Figure 3: Relative orbits in the x-y plane of the LVC frame when propagated using CW equations. These diagrams depict the effect of non-zero $x_d$ on the relative orbits. The $a_e$, $y_d$ and $\beta$ elements are also depicted.**

ROEs also simplify the propagation of relative orbits in the LVC, which is analogous to the simplification that KOEs afford in the ICRF. The propagation of the ROEs is similar to the propagation of position and velocity using the Clohessy-Wiltshire (CW) equations on linearized relative motion [3]. Under Clohessy and Wiltshire's assumption of a circular reference orbit, $a_e$, $x_d$, $z_{max}$ and $\gamma$ remain constant. $\beta(t)$ is propagated from $\beta(0)$ using Eq. 2:

$$\beta(t) = \beta(0) + \omega t \tag{2}$$

where $\omega$ is the mean motion of the circular reference orbit. Hence, $\beta$ is the phase angle of the relative orbit that results in the periodic angular motion. $y_d(t)$ is propagated from $y_d(0)$ using Eq. 3:

$$y_d(t) = y_d(0) - \frac{3}{2}\omega x_d t. \tag{3}$$

If $x_d = 0$, then there is no $y_d$ drift, and the relative orbit is closed as seen in Fig. 3a. When the energy of the two absolute orbits is not equal, $x_d \neq 0$, and secular drift in $y_d$ results as modeled in Eq. 3 and shown in Fig. 3b. The difficulty of maintaining two orbits with exact $x_d = 0$ motivates the concept of passive safety.

## 2.3. Definition of Passive Safety

It is extremely difficult (if not impossible) to equate the energies of two orbits when there is navigation and thruster noise in the systems. Therefore, two orbits will almost certainly have a non-zero $x_d$ with secular drift of $y_d$. If the guidance, navigation, and control malfunctions, then the $y_d$ drift will not be corrected at all. Therefore, the cluster of modules should maintain a passively safe configuration that prevents collisions when $y_d$ is not controlled. Because the $y_d$ drift is solely along the $y$-axis, this requirement equates to maintaining separation in the $x$-$z$ plane.

Figure 4 is the geometric interpretation of $a_e$, $\beta$, $z_{max}$, and $\gamma$ in the $x$-$z$ plane. Passive safety is defined using the minimum separation of two relative orbits in the $x$-$z$ plane of LVC. If the LVC frame is centered on one of the orbits, then it is defined as the minimum distance of ROEs from the origin. The sub-figures of Fig. 4 demonstrate the effect of different $\gamma$ values on the geometry of relative orbits in the $x$-$z$ plane. As $\gamma$ approaches 90° or 270°, the relative orbit will "tip over" itself in the $x$-$z$ plan and violate the rule of passive safety. Therefore, two orbits must meet the following conditions in order to remain passively safe: $\frac{a_e}{2} \gg r_1 + r_2$ and $z_{max}\sin(\gamma) \gg r_1 + r_2$ where $r_1$ and $r_2$ are the radii of the modules in the two orbits. These values should be significantly larger than $r_1 + r_2$ to provide a reasonable guarantee of passive safety. For an in-depth discussion of passively safe cluster design, the interested reader can reference Schmidt [19].

## 2.4. Secular Drift Due to J₂

Secular drift needs to be corrected periodically by station keeping in order to maintain the maximum inter-module distance (IMD) of the cluster. As long as $x_d$ is non-zero, the corresponding $y_d$ secular drift is much larger than the drift due to discarded nonlinear terms and higher order gravity terms due to non-spherical Earth. After non-zero $x_d$, the second zonal harmonic of gravitational forces due to non-spherical Earth ($J_2$) is the largest contributor to relative drift of two orbits. $J_2$ causes significant secular drift of $z_{max}$ and $a_e$, which must be corrected over time to maintain the

**(a)** $\gamma = 0°$ or $\gamma = 180°$     **(b)** $\gamma = 45°$, $\gamma = 135°$, $\gamma = 225°$ or $\gamma = 315°$     **(c)** $\gamma = 90°$ or $\gamma = 270°$
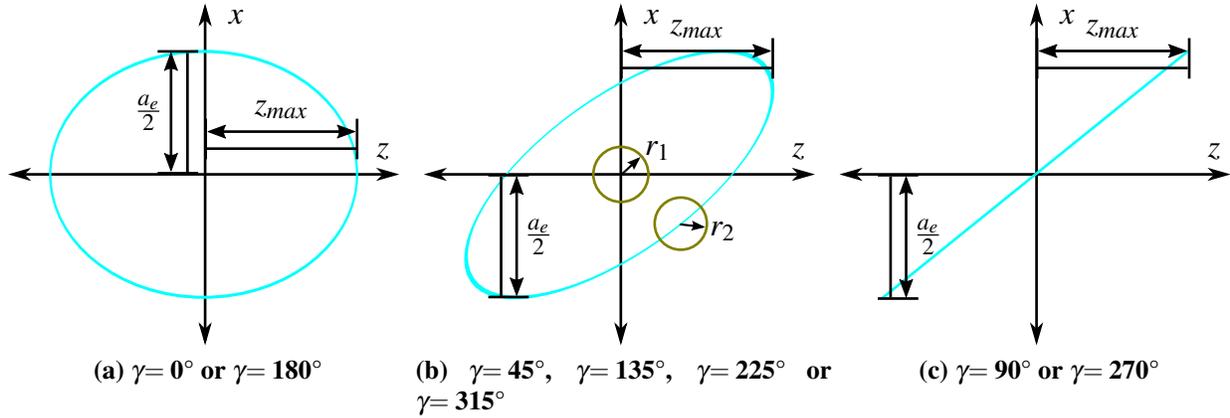
**Figure 4: Relative orbits in the x-z plane of the LVC frame when propagated using CW equations. These diagrams depict the effects of $a_e$, $z_{max}$ and $\gamma$ on the cluster. As $\gamma$ approaches 90° or 270°, the relative orbit is said to "tip over" on itself. The orbit is passively safe with respect to the origin when $a_e > 0$, $z_{max} > 0$, $\gamma \neq 90°$ and $\gamma \neq 270°$.**

cluster. $J_2$ also causes drift of $\gamma$ that threatens passive safety of the cluster. Research into $J_2$-invariant relative orbits has shown that two orbits on the same inclination do not have any secular drift in $z_{max}$ or $a_e$ [5, 2]. Therefore, the strategies discussed in this paper place a high priority on maintaining zero differential inclination. However, two orbits on the same inclination will still exhibit drift in $\gamma$, which needs to be corrected periodically.

### 3. Loop Closure of Maneuver Planning for Station-Keeping

All of the station-keeping strategies developed in this paper utilize a common algorithm for loop closure of maneuver planning. There are decision points in the algorithm that define the behavior of different strategies. Each strategy is defined by its method for deciding whether or not to generate new maneuver plans and its method for determining the target timing that it uses to plan maneuvers. These methods and the tuning parameters of the strategies are presented below, including a detailed discussion of using ROEs to define control boxes and to determine maneuver targets.

#### 3.1. Pseudo-Algorithm for Loop Closure of Maneuver Planning

The algorithm for loop closure of maneuver planning (LCMP) originates from the concept of receding horizon control (RHC). In its most basic form, LCMP is equivalent to RHC, but the more effective strategies deviate from true RHC to achieve desired performance characteristics.

The RHC problem is an optimal control problem solved repeatedly for a finite time window. As time progresses, each repetition of RHC has the same amount of finite time for the optimal control window. The significance of this is that the final time of the window is receding into the horizon. LCMP targets and maintains a desired relative orbit defined by a set of ROE, using state feedback from the navigation system to update maneuver plans in the same manner as RHC. The algorithm is implemented as a cyclic process as shown in Fig. 5. Each iteration of the algorithm is a control cycle. At the start of each cycle, the latest available state estimates from Navigation are used to
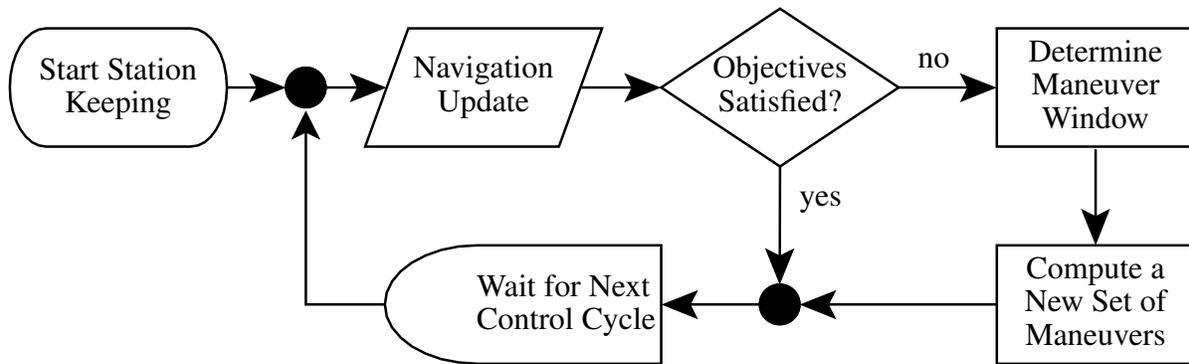
**Figure 5: Flow diagram for the LCMP algorithm. Different strategies have different control objects and different methods for determining the maneuver window.**

predict if the module's current set of maneuvers achieves the control objectives of the strategy for each module in the cluster.

For most of the strategies, the objective is defined as a control box that is defined by ranges of ROEs. To improve performance, the strategies are implemented using a leader-follower control architecture. At every check of the objectives, a leader is chosen for the cluster. Changing the leader frequently balances the fuel requirements across the cluster, but changing the leader too frequently can cause excessive trajectory corrections. The control box ROE ranges are computed and checked with respect to the current leader. If the objectives are not satisfied, then OMS requests a new set of maneuvers from Maneuver Planning Service (MPS) as shown in Fig. 1.

The request includes a list of modules that need new maneuver plans, a desired target (or target range), and a maneuver window for achieving that target. The decision process for determining the target and maneuver window is unique to each strategy. The algorithm used for optimal maneuver planning, which uses the Gim-Alfriend state transition matrix with linearized eccentricity and $J_2$ to solve the maneuver planning problem [20], and its implementation are detailed by Brown [16]. The algorithm computes a maneuver plan that achieves the target with minimal fuel consumption modeled as the total $\Delta V$ of all the maneuvers in the plan. After maneuver planning is complete, the algorithm pauses until the next control cycle.

### 3.2. Strategies for Control Objectives and Maneuver Windows

The primary inspiration for LCMP is Tillerson [4], who solves convex programs to achieve $\Delta V$ optimal maneuvers. For station-keeping, Tillerson uses an inner and outer control box. When the relative trajectory violates the outer control box, a $\Delta V$ optimal maneuver plan is solved that returns the module to the inner control box. LCMP can be configured similarly but offers more variety in its selection of maneuver windows and control objectives.

Figures 6 through 8 demonstrate the three different strategies for evaluating control objectives and determining maneuver windows. If the system does not have a strict convergence deadline, then the first strategy configures LCMP to use a receding horizon that conserves energy. Instead of evaluating control objectives, RHC requests a maneuver plan every control cycle as demonstrated in Fig. 6. Every control cycle uses the same maneuver window size, which causes the target
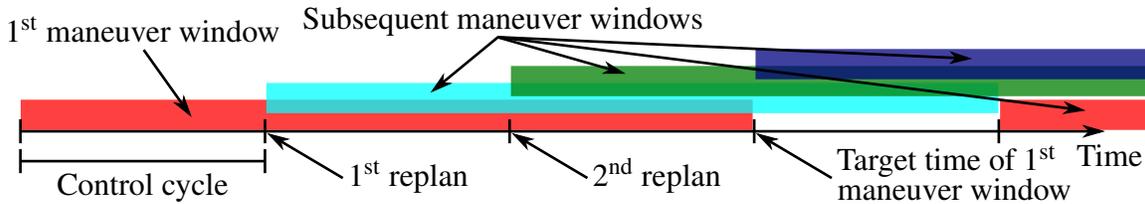
**Figure 6: Manuever windows for RHC. A new maneuver plan is created at every step of the control cycle, and the maneuver window recedes into the horizon over time.**
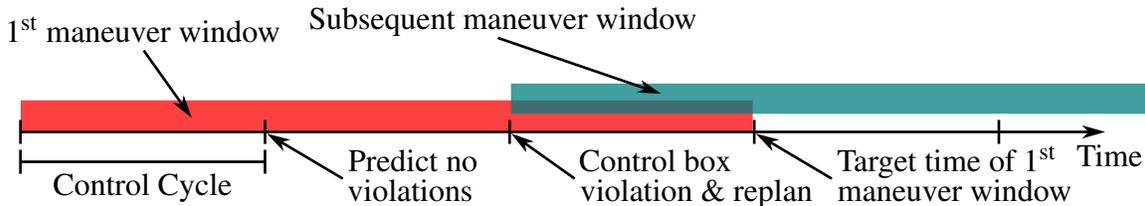


**Figure 7: Maneuver windows for pRHwCB. At every step of the control cycle, the module's latest state estimate and current maneuver plan are checked against its control box. If the control box is satisfied, then the current maneuver plan is deemed acceptable.**
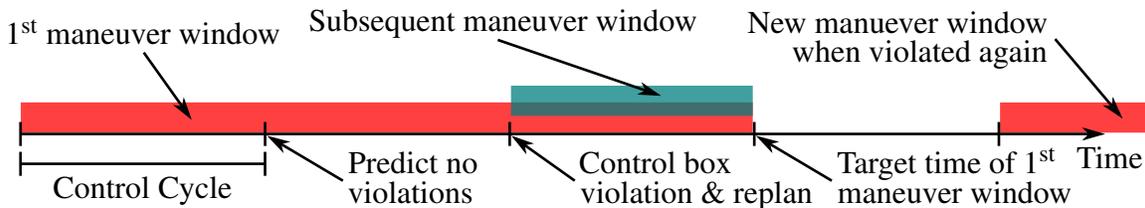


**Figure 8: Maneuver windows for FHwCB. If a control box is violated when there are no maneuver plans for that module, then a full maneuver window is used. If the module has a maneuver plan, then the new window has the same target time as the current maneuver plan.**

time to recede into the horizon. This implements traditional RHC, and could be proven to have guaranteed stability with a suitable maneuver planning subsystem by applying the methods in Mayne [13].

The second strategy is a modification to traditional RHC with the addition of control boxes. Figure 7 demonstrates LCMP with control boxes, which is named pseudo-receding horizon with control boxes (pRHwCB). If the current maneuver plan ends within the control box, then pRHwCB does not request a new maneuver plan. This approach has less frequent maneuvers when the minimum impulse requirement is large. pRHwCB can be configured with inner and outer control boxes like in Tillerson [4], but a single control box was found to be more effective. In an attempt to further reduce the maneuver frequency, fixed horizon control with control boxes (FHwCB) is introduced as the third strategy. FHwCB fixes the target time of subsequent maneuver plan windows to the target time of the first maneuver window. This essentially shrinks the size of the maneuver window of subsequent maneuver plans, which is demonstrated in Fig. 8. The computation of target ROEs within the control boxes for pRHwCB and FHwCB are discussed in the next section.
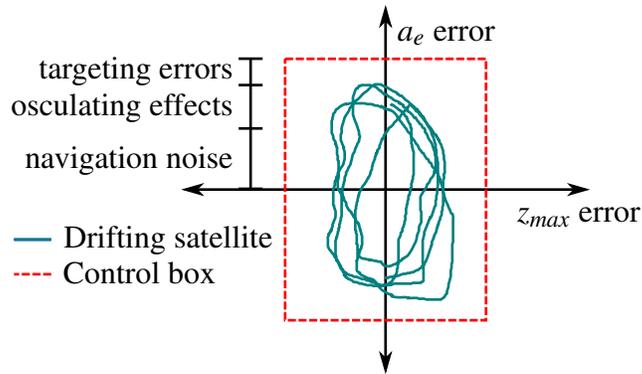
**Figure 9: Control box ranges for $a_e$ and $z_{max}$ with notional representation of relative motion in the plane. The ranges are selected based on the sum of navigation noise, osculating effects of Earth's gravity, and targeting errors.**

### 3.3. Using Relative Orbit Elements to Specify Targets and Control Boxes

LCMP uses ROEs to specify controller objectives in the form of control boxes and to specify target states. Station-keeping should be insensitive to noise and periodic disturbances while maintaining sensitivity to secular drifts that pull the cluster apart. Control boxes are essentially large deadbands that desensitize the controller to small perturbations but still allow the correction of larger secular drifts. Control boxes are defined as ROE ranges. The effects of ROE ranges are diagrammed by dividing the ROEs into three pairs. Each pair has distinct similarities that stand out when the pair is plotted on a two-dimensional plane.

Defining control boxes as ROE ranges offers several advantages over defining them as ranges on position and velocity. Although it is easy to specify polygons in the position and velocity space, the shape of relative orbits is not linear. A range of ROE better represents the non-linear space, which can wrap around the target relative orbit. Furthermore, determining the limits for control boxes on velocity is difficult. This section demonstrates that ROEs offer a convenient visualization of the control box for all six ROEs using three separate planes. It is also very convenient that $\beta$ is the only ROE that is changing over time. Therefore, the control box range for $\beta$ is the only range that needs to be parameterized by time. The ranges for all other ROEs can be time-invariant.

The first plane to be investigated contains $a_e$ and $z_{max}$. Figure 9 is an example of control box ranges for $a_e$ and $z_{max}$. There is no secular drift in $a_e$. Therefore, the $a_e$ range is chosen by adding navigation noise, osculating effects of higher order gravity, and targeting errors. If the cluster configuration places modules on the same inclination, then there will not be any drift in $z_{max}$. If the modules are placed on different inclinations, then the $z_{max}$ range should be designed with some additional buffer for the secular drifts. In addition, the $z_{max}$ target should be offset in the control box range so that the largest possible drift across the control box is obtained.

The second plane contains $\beta$ and $\gamma$. Figure 10 is an example of control box ranges for $\beta$ and $\gamma$. The linearized effects of J$_2$ cause a secular drift in $\beta$ and $\gamma$ at the same rate but in opposite directions, which is due to higher order gravity terms. To maintain the same inclination as the reference orbit
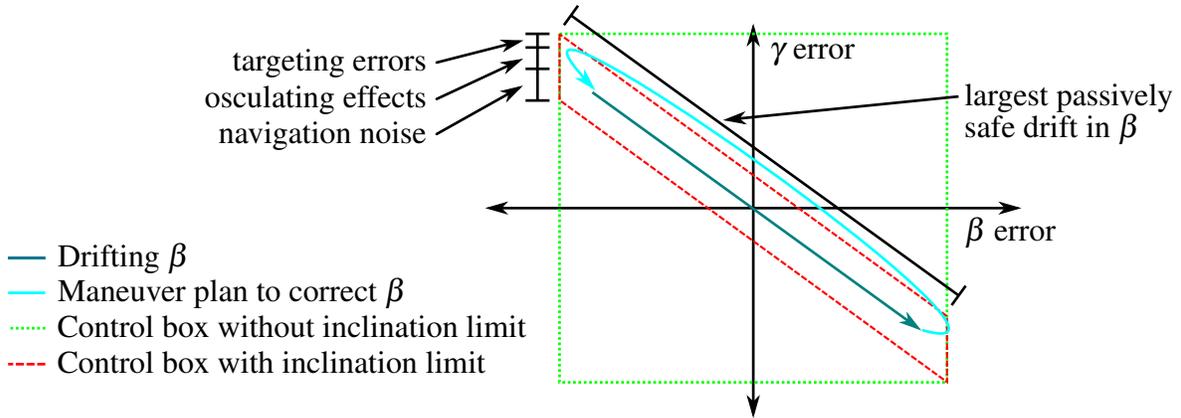
**Figure 10: Control box ranges for $\beta$ and $\gamma$ with a notional representation of relative motion in the plane. The ranges are coupled because $\beta$ and $\gamma$ have a secular drift at the same rate.**

the relationship

$$\beta + \gamma = \theta_{ref} \qquad (4)$$

must be maintained on average where $\theta_{ref}$ is the true argument of longitude of the reference orbit. The natural drift of $\beta$ (the Drifting $\beta$ arrow in Fig. 10) maintains this relationship. To prevent frequent burns, $\beta$ is allowed to drift as far as possible, without violating passive safety. If $\gamma$ were allowed an equal range, then Eq. 4 would be violated significantly at the far corners (dotted line in Fig. 10). Therefore, the control box around $\beta$ and $\gamma$ is designed as a parallelogram.

The third plane contains $x_d$ and $y_d$, which sees the most secular drift when $x_d \neq 0$. Two different methods can be used to control motion along this plane. The first method is the centering method, which Fig. 11 demonstrates. Natural motion causes the module to drift to the limits of $y_d$. When the limit is reached, the module is targeted back to the center of the control box for $y_d$ and to $x_d = 0$. Because navigation and guidance is not perfect, $x_d = 0$ will not be obtained exactly, and the process will continue. The second method is the bouncing method, which Fig. 12 demonstrates. Instead of targeting back to the center of the $y_d$ range and $x_d = 0$, this method purposely sets an $x_d$ offset that is large enough to guarantee that $y_d$ will drift in a certain direction. This method is more efficient for large $y_d$ ranges.

### 3.3.1. Maintenance of Equal Energy

The centering method and bouncing method for $x_d$ and $y_d$ control rely on accurate targeting of $x_d$. The target specified for $x_d$ is the desired semi-major axis difference of the target relative orbit with respect to the reference orbit. Unfortunately, higher order gravity terms cause periodic oscillations in the instantaneous semi-major axis of the module and reference. Therefore, the $x_d$ target should be the mean semi-major axis difference. Therefore, LCMP adjusts the instantaneous $x_d$ target so that the mean semi-major axis difference is correct.

The $x_d$ adjustment is accomplished by using an osculating to mean orbital element conversion [21]. To avoid the numerical inaccuracies that accumulate from transforming from ROE to LVC to ICRF to mean orbital elements to osculating orbital elements, and then back to ICRF, LVC and ROE, a shortcut is used that only adjust the $x_d$ ROE. $x_d$ is defined as the difference in semi-major axes.
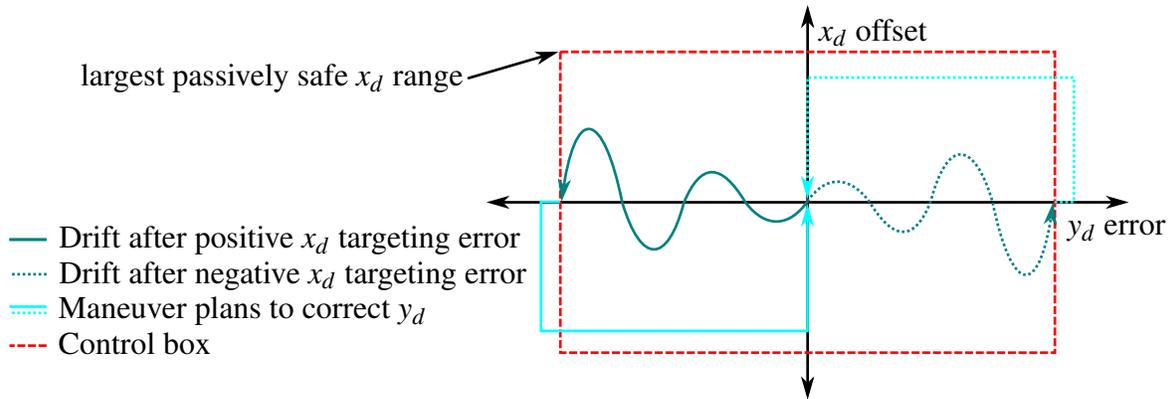
**Figure 11: Control box ranges for $x_d$ and $y_d$ using the centering method with a notional representation of relative motion in the plane. $x_d$ is targeted as close to zero as possible, and the module could drift forward or backward in $y_d$ depending on the $x_d$ targeting error.**
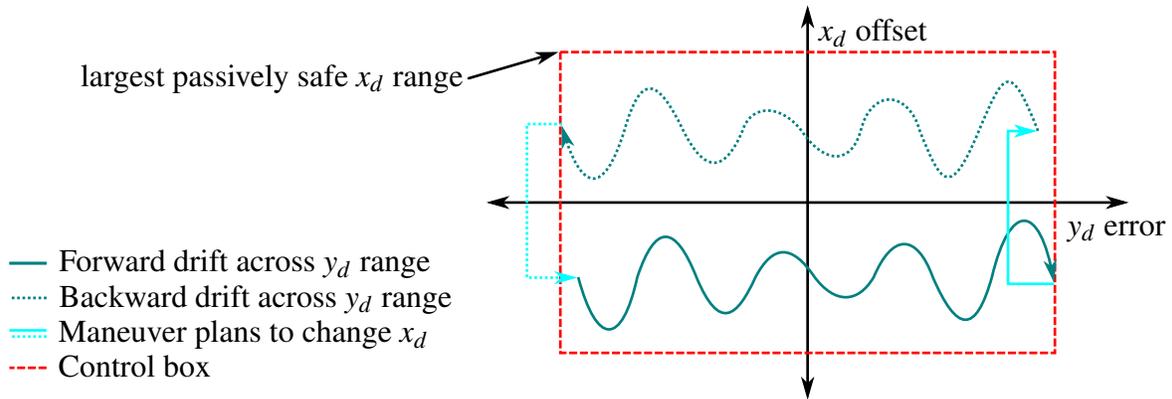


**Figure 12: Control box ranges for $x_d$ and $y_d$ using the bouncing method with a notional representation of relative motion in the plane. $x_d$ is targeted to a non-zero value that will force $y_d$ drift in a particular direction. On the other side of the control box, the $x_d$ target is negated.**

Therefore, the conversion is evaluated from ROE to LVC to ICRF to mean orbital elements to osculating orbital elements. The difference of the module mean semi-major axis and the reference mean semi-major axis is subtracted from the target instantaneous $x_d$.

### 3.4. Performance Tuning

LCMP has seven primary configurations summarized in Table 1. Configurations that showed poor performance during initial testing were removed before the Monte Carlo simulation. All configurations share three major tuning parameters. The most effective tuning parameter is the controller horizon length that determines how far into the future the algorithm is planning. Performance is also greatly affected by the control cycle of the algorithm, which determines how often the cyclic process repeats. The third major tuning parameter is the control box. It is also possible to tune the algorithm by introducing a minimum impulse that is larger than the actual minimum impulse of the propulsion method, but in practice the control box has been much more effective.
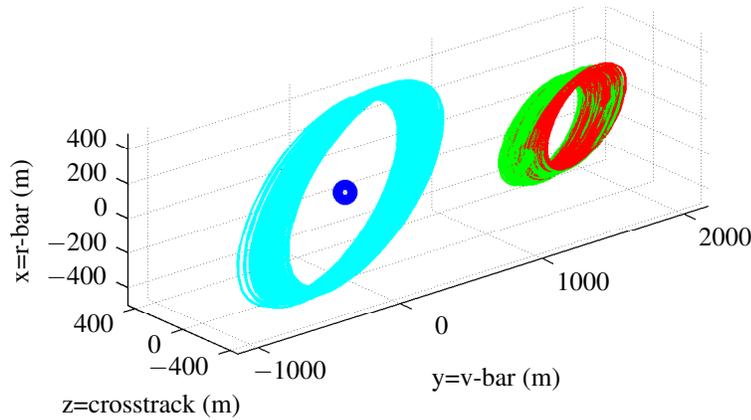
**Table 1: Summary of several strategies configured for station-keeping using LCMP.**

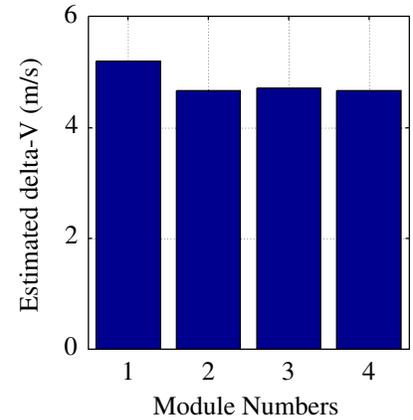| Strategy | Control Objective | Maneuver Window | Control Boxes | Targeting Method | Monte Carlo Performed |
|---|---|---|---|---|---|
| RHC | Always plan | Receding | None | Direct targeting | ✓ |
| pRHwCB Centering | ROE control box | Receding | Outer only | Center of control box | ✓ |
| pRHwCB Bouncing | ROE control box | Receding | Outer only | Bouncing inside control box | ✓ |
| pRHwCB Centering Inner/Outer | ROE control box | Receding | Inner and Outer | Center of control box | |
| FHwCB Centering | ROE control box | Shrinking | Outer only | Center of control box | ✓ |
| FHwCB Bouncing | ROE control box | Shrinking | Outer only | Bouncing inside control box | |
| FHwCB Centering Inner/Outer | ROE control box | Shrinking | Inner and outer | Center of control box | |

The control horizon is the most effective parameter for tuning the controller. A shorter horizon causes more frequent burns and larger total $\Delta V$, but reduces trajectory dispersions. A longer horizon will slightly reduce burn frequency, but it will also increase trajectory dispersions. See Fig. 13 for a four module example with a short horizon of 6 control cycle periods and Fig. 14 for an example with a long horizon of 12 control cycle periods. The control period is 1450 seconds, the thruster is 10 N and the control box is disabled. The results were obtained by simulating over 300 orbits with perfect navigation, and the $\Delta V$ results are extrapolated for a six month mission.

Reducing the control cycle period of LCMP increases the $\Delta V$. When LCMP checks maneuver plans too often, the targeting errors introduced by unmodeled dynamics and navigation noise will cause repeated planning and extra burns. A large control box can help to alleviate this problem, but it is not a cure. One should exercise caution when increasing the control cycle, because an increased control cycle can result in larger trajectory dispersions and even instability.

Tuning the control box is the least effective method for reducing $\Delta V$. However, it is absolutely critical for reducing burn frequency. A larger control box allows the modules to drift further before maneuvers are scheduled to return the module to its original position, which decreases burn frequency but results in much larger trajectory dispersions. Figure 15 provides an example with a large control box. The total $\Delta V$ over six months is larger than the previous example with the same horizon length of 12 control cycle periods, but burns occur less frequently at 11.4 orbits between burns instead of 6.6 orbits between burns without a control box.
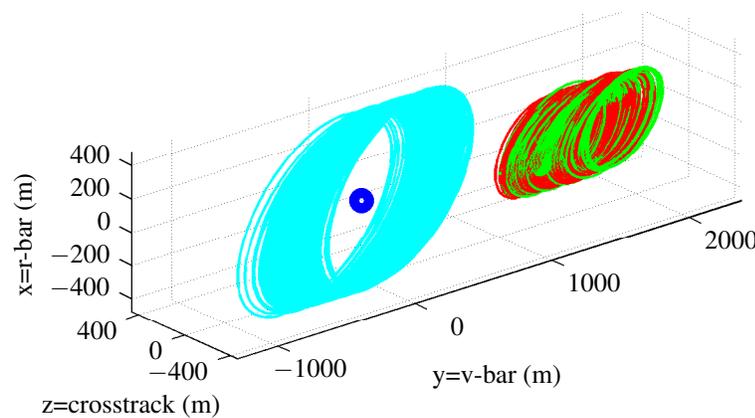
(a) Module trajectories in the LVC frame of the first module that demonstrate small trajectory dispersions. There are 2.8 orbits between burns.
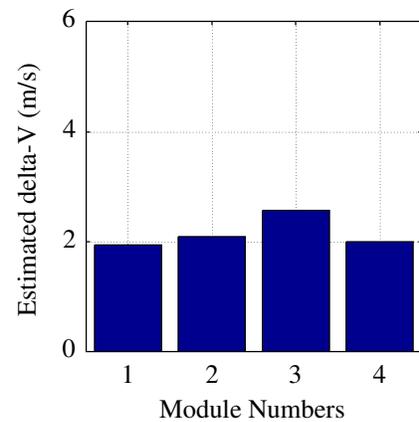
(b) Estimated total $\Delta V$ over six months for the cluster is 19.2 m/s.

**Figure 13: Station-keeping performance with control box disabled and a short horizon of 6 control cycle periods.**



(a) Module trajectories in the LVC frame of the first module that demonstrate medium trajectory dispersions. There are 6.6 orbits between burns.
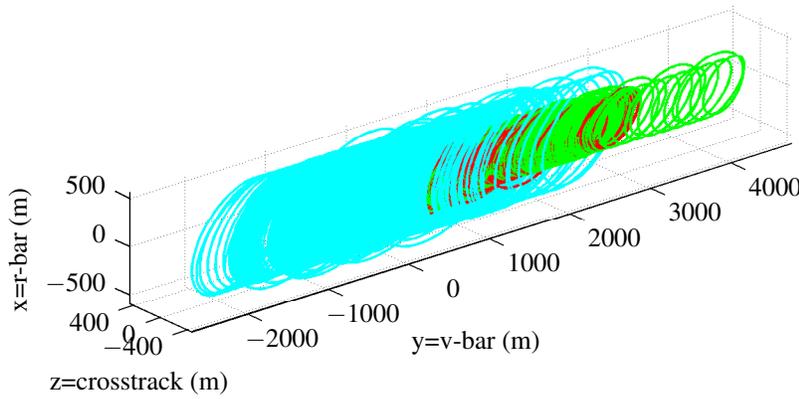
(b) Estimated total $\Delta V$ over six months for the cluster is 8.59 m/s.
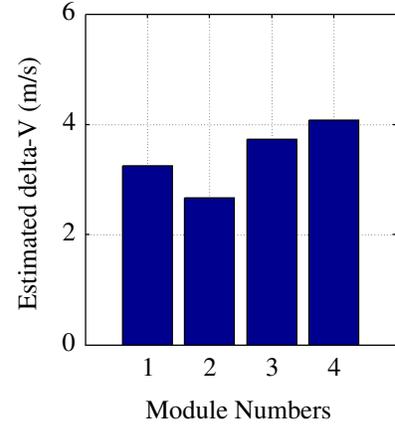
**Figure 14: Station-keeping performance with control box disabled and a long horizon of 12 control cycle periods.**

## 4. Review of the Flocking Controller for Station-Keeping

The flocking controller was first developed by Schwartz and Krenzke [6]. It is designed around the idea that a cluster of modules does not need to hold a formation in order to stay together. Instead of formation keeping, this controller aims only to keep the cluster together and maintain the modules in passively safe orbits while minimizing fuel use and burn frequency. Passive safety is parameterized by a safe zone size that is a distance to maintain separation in the *x-z* plane of LVC. Control of in-plane motion is performed by a proportional derivative (PD) controller with a deadband.

**(a) Module trajectories in the LVC frame of the first module that demonstrate large trajectory dispersions. There are 11.4 orbits between burns.**

**(b) Estimated total $\Delta V$ over six months for the cluster is 13.7 m/s.**

**Figure 15: Station-keeping performance with a control box that allows relative large along-track drift and horizon of 12 control cycle periods.**

The flocking controller will act to enforce a safety zone. The safety zone size determines the probability of collision and minimum safe distance permitted by the controller. However, a larger safety zone translates into a larger danger zone that requires larger burns for a module to transfer across the danger zone. To establish the safety zone, the flocking controller maintains three conditions between each pair of module ROEs. First, each pair's $z_{max}$ must be above a minimum boundary, which is set by the safety zone size. Second, each pair's $a_e$ must be above a minimum boundary, which is set by the safety zone size. Third, each pair's $\gamma$ must not be approaching 90° or 270°. More precisely, each neighbor's gamma value must be a certain angular distance away from 90° and 270°, and this angular distance is computed from the zone size and the pair's current $z_{max}$ and $a_e$. Corrections of $\gamma$ are made using a maneuver that is fired along the $y$ axis, $\Delta V_y$, which is computed from a relationship derived from Eq. 1:

$$\Delta \gamma = \arctan \left( \frac{\omega z_{max} \sin(\gamma + \beta + \omega t_b)}{\omega z_{max0} \cos(\gamma + \beta + \omega t_b)} \right) - \arctan \left( \frac{a_e \sin(\beta + \omega t_b)}{a_e \cos(\beta + \omega t_b) + \frac{4}{\omega} \Delta V_y} \right)$$

where $t_b$ is the time of the burn. The time of the maneuver is limited to perigee or apogee to minimize the size of the required $\Delta V$.

Corrections for along-track drift follow a PD control scheme. The controller observes the current $y_d$ and $y_d$ drift rate with respect to the leader module. Then, using a set of PD gains, it performs a burn that biases $x_d$ to correct the situation. The PD controller includes limits on $y_d$ and $x_d$, which are also used as tuning parameters. The $y_d$ limit is essentially a proportional saturation limit because it represents the maximum $y_d$ offset that will be used in the controller computation. The $x_d$ limit is essentially a deadband. It represents the minimum value of $x_d$ correction that will trigger a maneuver.

The PD burns and the $\gamma$ correction burns not only affect the intended ROEs, but also all other ROEs. Therefore, the PD controller verifies that a maneuver will not violate the safety zone of any

15

pair before the maneuver is scheduled. The PD controller and $\gamma$ correction also adhere to upper bounds on $a_e$ and $z_{max}$. Neither will schedule burns that violate these upper bounds.

## 5. Performance Analysis and Station-Keeping Results

Station-keeping performance is critical to guaranteeing the mission lifetime. The cluster will be performing station-keeping maneuvers for the majority of the mission, and fuel is a limited resource. If the station-keeping performance does not meet expectations, then the mission lifetime will be reduced accordingly. This section summarizes the key performance measures and performance tuning of LCMP. The differences between RHC, pRHwCB, FHwCB, and flocking controller are also discussed.

### 5.1. Mission Scenario

Station-keeping performance of a four module cluster is analyzed for a sun synchronous orbit. The parameters of the orbit are summarized in Table 2. Table 3 is the cluster configuration that was used for evaluation, which is plotted for a few orbits in Fig. 16. Each module has a GPS receiver, and they are using GPS filters for navigation as described by Schmidt [17]. The GPS filters are tracking the same GPS satellites to reduce relative navigation errors. The true gravity model is a 12x12 model. There is an exponential drag model that is inconsequential at an altitude of 500 km. The true thruster model is an RCS model with a short rise time and fall time. The thruster provides 70 N of force with a specific impulse (ISP) of 230 seconds. The minimum impulse provided by this thruster is 1.3 cm/sec. Although the simulation does not model attitude control, noisy burn directions are modeled. Thruster direction noise is a Gaussian distributed white noise in azimuth angle and elevation angle of the burn. The three-sigma value of the noise for each angle is six degrees, which is modeled from 2 degrees of sensor error plus 1 degree of deadband plus 3 degrees of alignment error. Guidance and control is using a $J_2$ gravity model in its computations.

**Table 2: Orbital parameters for station-keeping evaluation**

| Parameter | Value |
|---|---|
| altitude | 500 km |
| inclination | 98.2° |
| eccentricity | 0 |
| right ascension of the ascending node | 0° |
| argument of perigee | 0° |
| true anomaly at start | 0° |
| time at start (sec after J2000) | 134308851.184 |

Monte Carlo simulation was used to validate performance of the station-keeping method. Forty runs of 500 orbits were conducted for each configuration of the controllers. During every run, each module is the leader for 125 contiguous orbits to balance fuel. Each run uses a different stream of random numbers, which affects the navigation noise and thruster noise. In addition, the initial positions of the modules are randomized within the $\beta$-$\gamma$ and $x_d$ control boxes. Initial conditions for $\beta$ and $\gamma$ are still chosen so that modules start out on the same inclination.

**Table 3: Initial cluster configuration and ROE targets with four modules used to evaluate performance.**

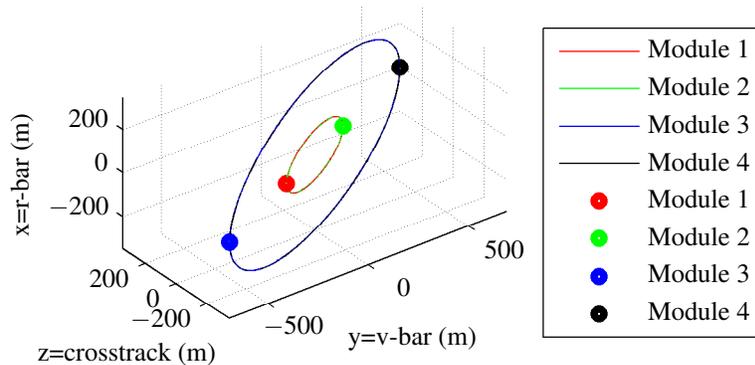|  | Module 1 | Module 2 | Module 3 | Module 4 |
|---|---|---|---|---|
| $a_e$ | 378 m | 378 m | 1073 m | 1073 m |
| $x_d$ | 0 m | 0 m | 0 m | 0 m |
| $y_d$ | 0 m | 0 m | 0 m | 0 m |
| $\beta$ | 270° | 90° | 270° | 90° |
| $z_{max}$ | 179 m | 179 m | 537 m | 537 m |
| $\gamma$ | 0° | 0° | 0° | 0° |



**Figure 16: Initial cluster configuration for station-keeping simulation, which is plotted in LVC for one orbit starting at the modules initial conditions.**

### 5.2. Performance Measures

The primary performance measure for station-keeping is total $\Delta V$ for station-keeping during the mission, which reflects the amount of fuel required. The following is a list of other performance measures, which usually conflict with minimizing $\Delta V$:

**Burn Frequency** Infrequent maneuvering is desirable to provide more opportunity for scientific studies, which may be interrupted while the module is slewing and accelerating.

**Burn Angles** The angles of burns are important when the mission requires the module to point at a specific attitude.

**Inter-module Distances** The minimum IMD and maximum IMD specified for the cluster should not be violated. In practice, noise and disturbances will cause violations of the minimum IMD. Therefore, significant violations of IMD were noted.

**Stability and Trajectories** The mission may require accurate tracking of the cluster configuration. In this case, minimizing dispersions from the nominal trajectory often requires more frequent burns that increase total $\Delta V$ over the module lifetime.

**Thruster Size** Although minimal station-keeping $\Delta V$ is more easily achieved using small, frequent burns, the F6 cluster required large thrusters to meet the requirements of a scatter maneuver during the mission. A large 70N thruster was used for these studies, which is a

thruster that is capable of achieving the scatter requirement [22].

## 5.3. Monte Carlo Simulation Results

Table 4 details the results of Monte Carlo simulation conducted for the study. CC is the control cycle in orbits, which is 0.5 orbit if not specified. MW is the maneuver window length in orbits. For example, RHC CC3 MW9 has a control cycle of three orbits and a maneuver window of nine orbits. pRHwCB Centering, 4km $y_d$, MW3 is using the centering method for $y_d$ control with a 4 km range across the $y_d$ control box and a control cycle of three orbits.

The 500 orbit $\Delta V$ number was extrapolated to estimate the $\Delta V$ for a six month mission. The three-sigma ($3\sigma$) value of the $\Delta V$ for six months over thirty runs is also listed. The ratio of the smallest six month $\Delta V$ to the largest six month $\Delta V$ also provides some indication of the variance in performance. Frequency of maneuvers is quantified by the average orbits between burns. Minimum and maximum IMD are sampled every 10 seconds, and the extreme values over 30 runs are tabulated. IMD in the $x$-$z$ plane is sampled every 60 seconds. Figure 17 and Fig. 18 visualize the $\Delta V$ consumption and the burn frequency results of the simulations, respectively. Probability of collision was computed using the covariance computed within the navigation filters, and it was zero for all cases.

**Table 4: Detailed results of Monte Carlo simulation for station-keeping strategies.**

| Controller | 6 mo. $\Delta V$ per Module (m/s) | 6 mo. $\Delta V$ $3\sigma$ value | Widest ratio of small:large $\Delta V$ | Ave. Orbits between Maneuvers | Min IMD (m) | Max IMD (m) | Min IMD $x$-$z$ plane (m) |
|---|---|---|---|---|---|---|---|
| RHC MW3 | 5.92 | 9.14 | 3.34:7.31 | 9.49 | 218 | 7,278 | 198 |
| RHC CC3 MW9 | 3.14 | 4.35 | 1.26:3.74 | 19.2 | 224 | 11,670 | 196 |
| pRHwCB Centering, 4km $y_d$, MW3 | 4.51 | 9.44 | 0.97:10.3 | 27.3 | 155 | 8,564 | 113 |
| pRHwCB Centering, 4km $y_d$, MW2 | 6.03 | 11.6 | 0.84:8.36 | 17.4 | 151 | 8,666 | 17 |
| pRHwCB Bouncing, 4km $y_d$, MW2 | 4.20 | 7.74 | 1.67:6.82 | 22.7 | 150 | 8,719 | 96 |
| FHwCB Centering, 4km $y_d$, MW3 | 4.83 | 8.33 | 1.71:6.27 | 23.1 | 94 | 8,517 | 80 |
| Flocking Controller | 10.4 | 38.4 | 1.17:23.2 | 19.7 | 76 | 18,565 | 74 |

RHC MW3 has acceptable $\Delta V$ performance over six months, but the burn frequency is very high at about one burn for every nine orbits. A wide range of tunings were attempted in order to reduce the burn frequency without increasing the six month $\Delta V$. The RHC CC3 MW3 tuning has
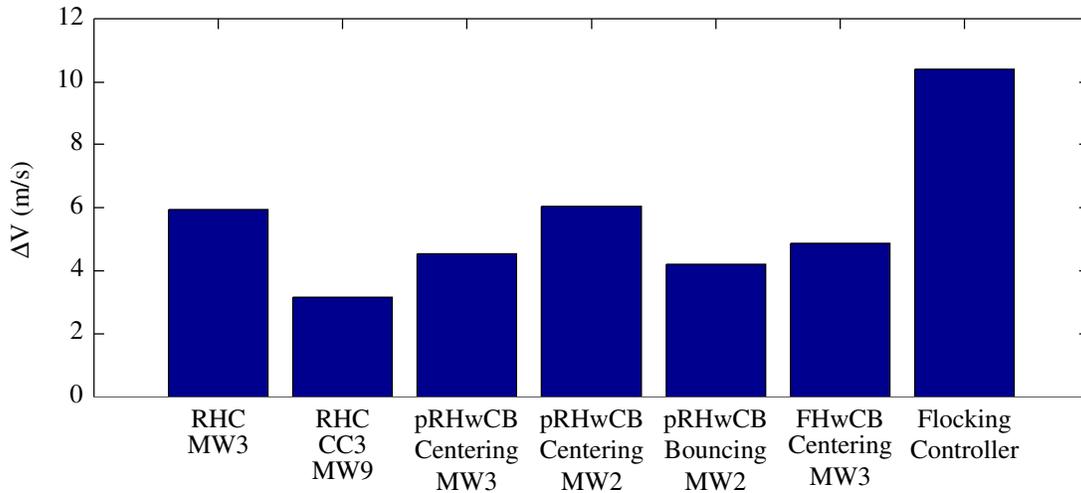
**Figure 17: Graphical $\Delta V$ summary for the station-keeping methods in Table 4.**
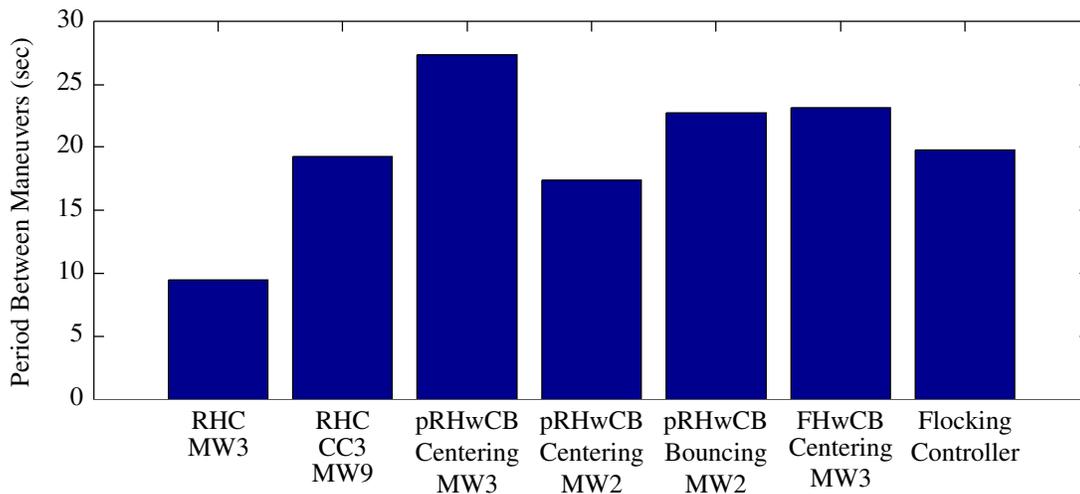


**Figure 18: Graphical burn frequency summary for the station-keeping methods in Table 4.**

a much lower burn frequency of one burn for every nineteen orbits, however, checking the orbits infrequently at a control cycle of three orbits can lead to stability issues. Although this tuning maintains a safe minimum IMD, the higher maximum IMD indicates that the dispersions from the target orbits are much larger than with RHC MW3. Therefore, in spite of the favorable numbers for the other performance measures, RHC CC3 MW3 is not recommended.

The control box approaches are the most stable, and they also have hard limits on the module positions during drift periods. Both pRHwCB and FHwCB maintain the cluster using small total $\Delta V$ and infrequent maneuvers. The only tuning of pRHwCB that had poor performance was Centering with MW2 where the short maneuver window of two orbits causes dangerous flybys when the modules return to the center of the $x_d$-$y_d$ control box. The modules use extra fuel to avoid these flybys at the last minute, which is reflected in the total $\Delta V$.

The results indicate that the flocking controller is least efficient, but the data in Table 4 does not

tell the entire story. For most runs, the flocking controller was efficient as indicated by the lower limit of the $\Delta V$ range, but it occasionally encountered problems finding efficient changes for $\gamma$. These few cases skew the results dramatically. In addition, flocking controller lacks differential inclination control. The effects of non-zero differential inclination build up over a 500 orbit simulation.

## 6. Conclusions

Ultimately, selection of a station-keeping strategy depends on the mission objectives and module capabilities such as mission-specific quiet periods, a required mission formation, or the minimum impulse of the thruster. Table 5 is a summary of advantages and disadvantages for each algorithm. A flexible strategy that is configurable for RHC, pRHwCB, and FHwCB is implemented in OMS as part of CFA. The centering and bouncing methods are also configurable. pRHwCB with centering is the most efficient station-keeping for the simulated mission, and it is the method that is currently being validated for long runs of CFA using a software in the loop simulation.

**Table 5: Summary of advantages for the investigated station-keeping strategies.**

| Algorithm | Advantages | Disadvantages |
|---|---|---|
| RHC | Consistent burn directions | Frequent replanning; Potential for high burn frequency; No guaranteed finite convergence time |
| pRHwCB | Only replans when necessary; Lower burn frequency than RHC; Flexible design (encompasses RHC) | Unpredictable maneuver windows; Less consistent burn directions; No guaranteed finite convergence time |
| FHwCB | Predictable maneuver windows; Flexible design | Inconsistent burn directions; Higher $\Delta V$ than RHC or pRHwCB |
| Flocking | Low burn frequency | No $a_e$, $z_{max}$, inclination control, or formation keeping; Single burn maneuvers |

The flocking concept could be a viable control strategy worth further R&D study, but the current implementation does not demonstrate enough performance improvement over the pRHwCB to warrant its use. A 'hybrid' controller was attempted that combines the pRHwCB method with rules of Flocking to determine $\gamma$. Testing of this controller in long simulations revealed several defects in the algorithms that have not been addressed. However, in theory a set of flocking rules should exist that would, at the very least, replicate the functionality of pRHwCB by considering the long-term effects of a chosen target $\gamma$. Such rules may also be able to take advantage of situations that allow for more $\gamma$ drift than passively safe control boxes would allow.

## 7. Acknowledgement

**Distribution Statement "A." (Approved for Public Release, Distribution Unlimited)**

The views expressed are those of the author and do not reflect the official policy or position of the Department of Defense or the U.S. Government.

## 8. References

[1] Brown, O., Long, A., Shah, N., and Eremenko, P. "System Lifecycle Cost Under Uncertainty as a Design Metric Encompassing the Value of Architectural Flexibility." *AIAA SPACE 2007 Conference & Exposition*. Long Beach, CA, September 2007.

[2] Schaub, H. and Alfriend, K. T. "J2-Invariant Relative Orbits for Spacecraft Formations." *Celestial Mechanics and Dynamical Astronomy*, Vol. 79, No. 2, 2001, pp. 77–95.

[3] Clohessy, W. H. and Wiltshire, R. S. "Terminal Guidance System for Satellite Rendezvous." *Journal of the Aerospace Sciences*, Vol. 27, No. 9, 1960, pp. 653–658.

[4] Tillerson, M., Inalhan, G., and How, J. "Co-ordination and Control of Distributed Spacecraft Systems Using Convex Optimization Techniques." *International Journal of Robust and Nonlinear Control*, Vol. 12, No. 2-3, 2002, pp. 207–242.

[5] Vadali, S. R., Sengupta, P., Yan, H., and Alfriend, K. T. "Fundamental Frequencies of Satellite Relative Motion and Control of Formations." *Journal of Guidance, Control, and Dynamics*, Vol. 31, No. 5, September–October 2008, pp. 1239–1248.

[6] Schwartz, J. and Krenzke, T. "The Flocking Controller: A Novel Cluster Control Strategy for Space Vehicles." *AIAA Guidance, Navigation, and Control Conference*. No. AIAA-2013-4543, Boston, MA, August 2013.

[7] Lovell, T. A. and Tragesser, S. G. "Guidance for Relative Motion of Low Earth Orbit Spacecraft Based on Relative Orbit Elements." *AIAA/AAS Astrodynamics Specialist Conference and Exhibit*. Providence, RI, August 2004.

[8] Schwartz, J. and Krenzke, T. "Error-Contracting Impulse Controller for Satellite Cluster Flight Formation." *AIAA Guidance, Navigation, and Control Conference*. No. AIAA-2013-4541, Boston, MA, August 2013.

[9] Breger, L. and How, J. P. "Gauss's Variational Equation-Based Dynamics and Control for Formation Flying Spacecraft." *Journal of Guidance, Control, and Dynamics*, Vol. 30, No. 2, 2007, pp. 437–448.

[10] Vadali, S. R., Yan, H. and Alfriend, K. T., "Formation Maintenance and Fuel Balancing for Satellites with Impulsive Control." *AIAA/AAS Aerodynamic Specialist Conference and Exhibit*. Honalulu, HI, August 2008.

[11] Larsson, R., Berge, S. Bodin, P., and Jonsson, U., "Fuel Efficient Relative Orbit Control Strategies for Formation Flying and Rendezvous within PRISMA." *Advances in the Astronautical*

*Sciences*, Vol. 125, 2006, pp. 25.

[12] Rawlings, J. "Tutorial Overview of Model Predictive Control." *IEEE Control Systems*, Vol. 20, No. 3, 2000, pp. 38–52.

[13] Mayne, D., Rawlings, J., Rao, C., and Scokaert, P. "Constrained Model Predictive Control: Stability and Optimality." *Automatica*, Vol. 36, No. 6, 2000, pp. 789–814.

[14] Saponara, M., Barrena, V., Bemporad, A., Hartley, E., Maciejowski, J., Richards, A., Tramutola, A., and Trodden, P. "Model Predictive Control Application to Spacecraft Rendezvous in Mars Sample Return Scenario." *Progress in Flight Dynamics, Guidance, Navigation, Control, Fault Detection, and Avionics*, Vol. 6, December 2013, pp. 137–158.

[15] Hur-Diaz, S. and O'Connor, B. "Cluster Flight Application On System F6." *The 24th International Symposium on Space Flight Dynamics*, Laurel, MD, May 2014.

[16] Brown, A., Ruschmann, M. C., Duffy, B., Ward, L. Hur-Diaz, S., Ferguson, E., and Stewart, S. M., "Simulated Annealing Maneuver Planner for Cluster Flight." *The 24th International Symposium on Space Flight Dynamics*. Laurel, MD, May 2014.

[17] Schmidt, J. and Phillips, M. "A Distributed, Redundant Navigation and Fault Detection System for DARPA System F6." *AIAA Guidance, Navigation, and Control Conference*. No. AIAA-2013-4963, Boston, MA, August 2013.

[18] Hill, G., "Researches in the Lunar Theory." *American Journal of Mathematics*, Vol. 1, No. 1, 1878, pp. 5–26.

[19] Schmidt, J., Phillips, M., and Ruschmann, M. "Satellite Cluster Flight Design Considerations." *The 24th International Symposium on Space Flight Dynamics*. Laurel, MD, May 2014.

[20] Gim, D.-W. and Alfriend, K. T. "State Transition Matrix of Relative Motion for the Perturbed Noncircular Reference Orbit." *Journal of Guidance, Control, and Dynamics*, Vol. 26, No. 6, 2003, pp. 956–971.

[21] Cain, B. J. "Determination of Mean Elements for Brouwer's Satellite Theory." *The Astronomical Journal*, Vol. 67, No. 6, August 1962, pp. 391.

[22] Duffy, B., Brown, A., Ruschmann, M. C., Pinon III, E., and Ward, L. "Scatter Strategies for Cluster Flight." *The 24th International Symposium on Space Flight Dynamics*. Laurel, MD, May 2014.